ANNALS of Clinical and Translational Neurology
Open Access
ANA American Neurological Association since 1875

RESEARCH ARTICLE

Evaluation of disease progression in INCL by MR spectroscopy

Eva H. Baker[1], Sondra W. Levin[2,3], Zhongjian Zhang[2] & Anil B. Mukherjee[2]

[1]Department of Radiology and Imaging Sciences, Clinical Center, National Institutes of Health, Bethesda, Maryland, USA 20892
[2]Program on Developmental Endocrinology and Genetics, Eunice Kennedy Shriver National Institute of Child Health and Human Development, NIH, Bethesda, Maryland, USA 20892
[3]Department of Pediatrics, Walter Reed National Military Medical Center, Bethesda, Maryland, USA 20889-5600

Correspondence
Eva H. Baker, building 10, room 1C351, 9000 Rockville Pike, Bethesda, MD 20892.
Tel: 301-594-6175; Fax: 301-402-0882;
E-mail: bakere@mail.nih.gov

Funding Information
This project was supported entirely through intramural funding at the National Institutes of Health: INCL patients were studied under protocol 01-CH-0086 and NPC patients were studied under protocol 06-CH-0186.

Received: 7 May 2015; Accepted: 13 May 2015

Annals of Clinical and Translational Neurology **2015; 2(8): 797–809**

doi: 10.1002/acn3.222

Abstract

Objective: Infantile neuronal ceroid lipofuscinosis (INCL) is a devastating neurodegenerative storage disease caused by palmitoyl-protein thioesterase-1 deficiency, which impairs degradation of palmitoylated proteins (constituents of ceroid) by lysosomal hydrolases. Consequent lysosomal ceroid accumulation leads to neuronal injury. As part of a pilot study to evaluate treatment benefits of cysteamine bitartrate and *N*-acetylcysteine, we quantitatively measured brain metabolite levels using magnetic resonance spectroscopy (MRS). **Methods**: A subset of two patients from a larger treatment and follow-up study underwent serial quantitative single-voxel MRS examinations of five anatomical sites. Three echo times were acquired in order to estimate metabolite T2. Measured metabolite levels included correction for partial volume of cerebrospinal fluid. Comparison of INCL patients was made to a reference group composed of asymptomatic and minimally symptomatic Niemann-Pick disease type C patients. **Results**: In INCL patients, *N*-acetylaspartate (NAA) was abnormally low at all locations upon initial measurement, and further declined throughout the follow-up period. In the cerebrum (affected early in the disease course), choline and myo-inositol were initially elevated and fell during the follow-up period, whereas in the cerebellum and brainstem (affected later), choline and myo-inositol were initially normal and rose subsequently. **Interpretation**: Choline and myo-inositol levels in our patients are consistent with patterns of neuroinflammation observed in two INCL mouse models. Low, persistently declining NAA was expected based on the progressive, irreversible nature of the disease. Progression of metabolite levels in INCL has not been previously quantified; therefore the results of this study serve as a reference for quantitative evaluation of future therapeutic interventions.

Introduction

Neuronal ceroid lipofuscinoses (NCL)[1–3] are a group of neurodegenerative lysosomal storage disorders that are also known as Batten disease.[4–7] Fourteen NCL phenotypes have been identified; genes for 13 of these have been identified so far.[8,9] The infantile type, infantile NCL (INCL),[10] is caused by inactivating mutations in the *Cln1* gene,[11] which encodes palmitoyl-protein thioesterase-1 (PPT1).[11] Relative to most other NCLs, INCL has an early age of onset and more rapid progression. Children with INCL appear normal at birth, but by 11–18 months of age they manifest psychomotor retardation, myoclonus, and seizures followed by progressive loss of developmental milestones. By 2 years of age they are completely blind due to retinal degeneration. At around 4 years of age, these children fail to show any electrical activity measured by electroencephalography (including visual evoked potentials)[12] and remain in a persistent vegetative state until death. These grim facts underscore the desirability of developing an effective therapy for this disease.

The pathological findings include accumulation of intracellular autofluorescent material (ceroid), rapidly progressive brain atrophy resulting predominantly from loss of cortical neurons in the cerebrum, and neuroinflammatory findings. The accumulation of ceroid is a characteristic pathological finding in all NCLs.[1,2] Although the components and ultrastructure of the storage material vary across the different types of NCLs, electron microscopic analyses of the brain and other tissues from INCL patients show characteristic granular osmiophilic deposits (GRODs).[13,14]

Previous studies in cell cultures derived from INCL patients demonstrated that phosphocysteamine had a beneficial effect on the cell culture, resulting in depletion of intralysosomal ceroid deposits and suppression of apoptosis.[15] *N*-acetylcysteine, a potent antioxidant, has been reported to have beneficial effects on other neurogenerative diseases.[16] Because INCL is a rare disease (1 in >100,000 births) with a short life expectancy, recruitment of a large study group is impractical; this consideration, together with promising results from cell culture experiments, led to a "compassionate use" type of experimental design in which all patients received treatment with cysteamine bitartrate (Cystagon) and *N*-acetylcysteine (Mucomyst), without a control group, with the intention of comparing to the natural history and to future treatment interventions using quantifiable measures. These included behavioral and developmental assessments, EEG, ERG, magnetic resonance imaging (MRI)-derived brain volume measurements, and quantification of intralysosomal ceroid deposits. Toward the end of the study's recruitment period, quantitative magnetic resonance spectroscopy (MRS) was added to the quantifiable measures. Recently, an overview of the study results has been published[17]; the current report details the quantitative MRS findings.

Methods

MRS

A total of 10 patients were recruited for the study[17] (ClinicalTrials.gov number NCT00028262). The last two patients to enter the study (1M, 1F) had detailed quantitative ^{1}H-MRS exams performed in addition to clinical MRI exams that were performed on all participants in the study. The examinations of these two patients were acquired on a 3T Philips Intera (Philips Healthcare company, Best, Netherlands.) scanner using an eight-channel SENSE head coil. The MRI exam included 3D-MPRAGE images that were reformatted into three planes and used to guide prescription of the spectroscopy voxels. Single voxel spectroscopy was performed on voxels graphically prescribed from the MPRAGE images (PRESS localization; CHESS water suppression; TE = 38, 140, and 280 msec; TR = 2000 msec; 128 NEX). An unsuppressed water spectrum (TR = 5000 msec, TE = 38 msec, 16 NEX) was also acquired for each voxel. Identical gain and shim settings were used for all voxels obtained from the same prescription. Five voxel locations were acquired during each exam: pons, left thalamus, left cerebellar white matter (LCWM), left centrum semiovale (LCSO), and midline parietal gray matter (PGM). Typical voxel size was ~21 × 19 × 17 mm (range = 4.5–9.6 cm^3, mean = 6.8 cm^3), although the dimensions were adjusted to match the size and shape of the targeted anatomical area. In order to correct for cerebrospinal fluid (CSF) included within the voxels, we acquired a heavily T2-weighted image with location and slice thickness corresponding to the location of each MRS voxel (FSE; ETL = 8; TE = 500 msec; TR = 3000 msec). A phantom containing water was placed beside the head and included in the field-of-view of the CSF correction image. Treatment with cysteamine bitartrate and *N*-acetylcysteine was initiated after acquisition of baseline MRI and ^{1}H-MRS. Follow-up intervals for the INCL patients ranged from 6 to 12 months; the female patient was scanned five times and the male patient was scanned four times.

Reference group

Due to the unlikelihood of obtaining Institutional Review Board (IRB) approval to perform sedated scans on normal young children and the impracticality of obtaining high-quality images and spectra without sedation, a near-normal reference group was used. The reference group included children from 1 to 16 years old. These children were participants in a study of the natural history of Niemann-Pick disease type C (NPC) who were confirmed to have the gene, but were either asymptomatic or minimally symptomatic (a score of 0–5 on the NPC clinical severity scale[18]); sedated MRI and ^{1}H-MRS exams were routinely part of the NPC natural history study. MRI and ^{1}H-MRS acquisitions and postprocessing were identical in the INCL patients and in the reference group, except that multiple echo times for T2 measurement were not acquired as part of every exam for the reference group.

MRS postprocessing

Raw data for the 38 msec echo time were exported to LCModel.[19] The LCModel software automatically performs phase adjustments, ppm shift, baseline subtraction, and eddy current correction. Relative metabolite concentrations (and their uncertainties) are estimated by fitting the spectrum to a basis set of spectra. The unsuppressed water spectrum is then used to normalize the initial fit to generate a first estimate of metabolite concentration in the tis-

sue. The first estimates were corrected for estimated concentration of water within the tissues (varies according to whether the tissue is white matter [WM] or gray matter [GM]) and T1 of the metabolites within the tissues, using assumptions based on values published in the literature.[20] The spectroscopic peaks we analyzed were the *N*-acetylaspartate + *N*-acetylaspartyl glutamate (NAA + NAAG) peak at 2.0 ppm (for simplicity, hereinafter referred to as NAA), creatine peak at 3.0 ppm, choline-containing compounds at 3.2 ppm (hereinafter referred to as choline), myo-inositol peak at 3.5 ppm, and glutamine + glutamate + GABA (gamma-aminobutyric acid) peak at 2.2–2.4 ppm (hereinafter referred to as Glx). The T1 relaxation times that we used in our calculations were: T1 (NAA) = 1860 msec, T1 (choline) = 1320 msec, T1 (creatine) = 1740 msec, T1 (myo-inositol) = 1030 msec, and T1 (Glx) = 1230 msec.

CSF correction

Correction for partial volume of CSF included within the MRS voxel was performed as described previously.[21,22] Briefly, a very long TE, heavily T2-weighted image was acquired with the same orientation and center as the spectroscopy voxel, with the slice thickness matching the thickness of the spectroscopy voxel. A water phantom was placed within the field of view. Placing a region of interest (ROI) on the image corresponding to the voxel location and summing the values within the ROI effectively integrates the amount of CSF within the voxel, which is normalized by comparison to an ROI placed within the phantom. Depending on the voxel size and location, CSF correction in normal volunteers and in patients without atrophy is usually a matter of less than 5%, but due to the extreme atrophy in the INCL patients, CSF partial volume in this experiment reached as high as 46%.

T2 measurements

Water-suppressed spectra were acquired at each location with three different echo times: 38, 140, and 280 msec; all other acquisition parameters (including shim, water suppression, transmit gain, and receiver gain) were maintained the same for all three acquisitions. All three spectra were processed through the scanner's built-in spectroscopy package (Philips SpectroView analysis software Philips Healthcare company, Best, Netherlands.) using short TE peak models, resulting in an integral of the area under the curve for each peak. A linear regression was then performed on the natural log of each sequence of three areas, resulting in an estimate of the T2 for each metabolite peak. This calculation was performed only for the primary peaks of NAA, creatine, and choline, as the secondary peaks of these metabolites and also the multiplet peaks of myo-inositol, lactate, and Glx did not have sufficient signal to noise ratio (SNR) (particularly at TE = 280 msec) to perform this analysis. Plotting the T2 of each metabolite against the patient's age demonstrated that T2 varies not only by location, but also as a function of age for both the INCL patients and the reference group. In general, the T2 of all metabolites shortened with age, but the rate of shortening was more pronounced in the INCL patients. Due to the level of uncertainty in the individual measurements, a curve was fit to the measurements for each metabolite at each location, and the expected value derived from the curve was used for the T2 correction of each quantitative metabolite measurement; doing this also allowed us to use reference metabolite measurements that did not have a simultaneously acquired T2 measurement.

Reference curve for normal metabolite levels

Previous studies[23–27] have demonstrated that both ratios and actual concentrations of the ^{1}H-MRS visible metabolites change over time in the maturing brain, and that the changes are the most rapid in the youngest children. The levels are fairly stable in the age range of about 20–50 years.[21,24,27,28] Mathematically, the childhood portion of this pattern is fairly well approximated by a power curve (of the form $y = Ax^{B}$), and so for each metabolite at each location, a power curve was fit to the measurements of the reference group in order to generate a reference curve.

Statistical tests

To compare the metabolite ratios in the INCL patients relative to the reference measurements, a two-tailed, unequal-variance *T*-test was performed for each metabolite ratio at each location; a *P*-value ≤ 0.05 was considered to be statistically significant. Pearson's correlation coefficient (r) was calculated for each of the curve fits. No particular cut-off was used for r.

Results

Demographics

The female patient was scanned a total of five times in a span of 35 months. A total of 25 voxels had valid metabolite measurements, but only 20 had valid T2 calculations for all metabolites. (Due to the very low levels of metabolites measured at some locations in the later follow-up exams, the metabolite signal was not higher than the noise level in the TE = 280 msec spectra, and therefore the

calculation could not be made.) The male patient was scanned a total of four times in a span of 27 months. A total of 20 voxels had valid T2 calculations, but only 19 had valid quantitative metabolite measurements (the result of a technical failure generating an invalid unsuppressed water reference spectrum). The reference group contained 16 unique patients (8F, 8M) ranging in age from 1 to 16 years (mean = 4 years); 94 voxels had valid T2 measurements, and 121 had valid metabolite measurements.

T2 measurements

Measurements of metabolite T2 for the INCL patients and the reference group are plotted in Figure 1; the regression curves fitted to the measurements were subsequently used to correct the metabolite measurements for T2 decay. Selected points on the regression curves are presented in Table 1. In most cases, the T2 curve in the INCL patients is lower than the T2 curve in the reference group, indicating a shorter T2 for the same age; in the rest of the cases, the T2 curves overlap and are effectively the same. The pathophysiology of INCL does not seem to result in lengthening of metabolite T2 at any of the locations that we studied. At most locations for most metabolites, for both the reference group and the INCL patients, T2 becomes shorter with age. In the reference group, the change is generally small over this age range, with the exception of choline in the white matter (LCSO and LCWM) and all 3 metabolites in the left thalamus. However, for the INCL patients, some of the metabolites at some of the locations had rather dramatic changes in metabolite T2 with age. For example, NAA at all locations except the pons, creatine in the LCWM, and choline in the white matter (LCSO and LCWM) all demonstrated large changes in metabolite T2 with age.

NAA

Compared to the references, NAA for the INCL patients was lower at all five locations (Figure 2, right column). While NAA in the references increased with age at all five locations, NAA in the INCL patients dropped. The most extreme deficit of NAA was found in the PGM, followed closely by the LCSO. The deficit of NAA was less pronounced in the left thalamus, while deficits were least (but still clearly present) in the LCWM and pons. The best fit curves describing the trajectory of NAA in the INCL patients are given in Table 2.

Glutamine, glutamate, and GABA

The pattern of Glx in the INCL patients (Figure 3, right column) compared to the reference group generally parallels the findings in NAA, but the trends are weaker and the differences between the INCL and reference groups are less obvious, at least in part due to the greater uncertainty in the Glx measurements. Glx deficit was the greatest in the PGM, almost as large in the left thalamus, and least in the LCSO and pons. Glx seemed relatively normal in the LCWM.

Creatine

Creatine in the reference group was essentially stable for this age range (Figure 2, middle column). In the INCL patients, creatine in the PGM was initially low and declined progressively. The pattern was the same in the left thalamus, but with a smaller initial deficit and a more rapid decline. In the LCSO, creatine was initially normal but later declined. Creatine in the pons was normal. Creatine in the LCWM was either normal or perhaps slightly elevated. The creatine pattern is generally parallel to the pattern in NAA and Glx, but with a temporal lag.

Choline

In the reference group, choline measurements showed little variation with age over the age range of the study, although there was a slight rise in choline between childhood and adulthood that is not illustrated in the figure. The amount of choline in the INCL patients relative to the reference group varied depending on the location (Figure 2, left column). In the PGM and left thalamus, choline was low and falling. In the LCSO, choline was initially slightly high and later fell into the normal range. In the LCWM, choline was initially normal and later rose to be higher than normal. In the pons, choline was initially slightly low and later rose into the normal range.

Myo-inositol

Like choline and creatine, myo-inositol in the reference group was essentially unchanged over the age range of the study. The level of myo-inositol in the INCL patients relative to the reference group varied by location and demonstrated temporal evolution (Figure 3, left column). Myo-inositol was low in the PGM. Myo-inositol was high in the left thalamus and LCSO, appearing to reach a peak between 4 and 5 years of age. Myo-inositol was initially normal in the LCWM and pons, later rising above normal first in the LCWM and later in the pons.

Relationships between the metabolites

Relationships between the metabolites are plotted in Figure 4. NAA, Glx, and creatine are all linearly related to each other. The plots demonstrate that in GM, the drop

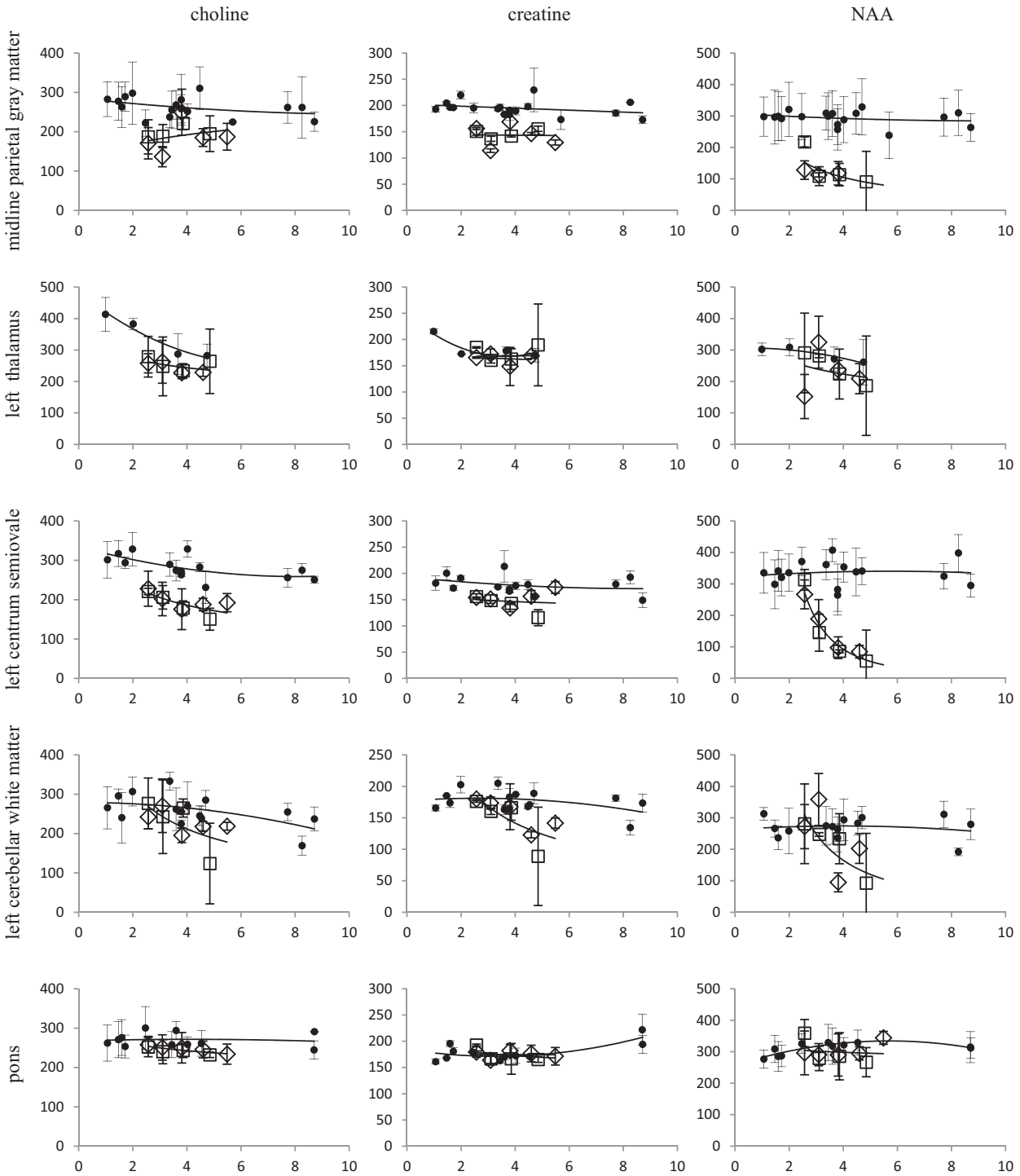

Figure 1. T2 measurements, comparison of infantile neuronal ceroid lipofuscinosis (INCL) patients to the reference group. Squares and diamonds represent the individual INCL patients, while circles represent the reference group. In general, the T2 of the metabolites decreases with age for both the reference group and the INCL patients, but the decline is faster for the INCL patients. In such a situation, failing to correct for the relative difference in T2 would exaggerate the measured metabolite deficits in the INCL patients (shorter T2 simulates a lower metabolite signal when not included in the calculation). On all plots, the horizontal axis is age (in years) and the vertical axis is the T2 relaxation time of the main metabolite peak (in msec).

Table 1. Comparison of calculated T2 decay constants (in msec).

	Choline			Creatine			NAA		
	Age 2	Age 4	Age 6	Age 2	Age 4	Age 6	Age 2	Age 4	Age 6
PGM									
Reference	267	256	245	178	193	189	302	294	285
INCL	169	192	208	146	144	143	188	104	75
LTHAL									
Reference	374	297	220	192	173	154	297	271	246
INCL	273	244	228	166	170	173	280	227	196
LCSO									
Reference	305	288	270	184	181	178	335	330	324
INCL	234	187	160	152	146	143	501	93	34
LCWM									
Reference	276	261	246	180	175	170	287	282	278
INCL	280	221	163	192	148	103	442	165	93
PONS									
Reference	266	265	264	171	178	186	288	281	274
INCL	257	244	230	182	172	167	308	298	293

NAA, *N*-acetylaspartate; PGM, parietal gray matter; INCL, infantile neuronal ceroid lipofuscinosis; LTHAL, left thalamus; LCSO, left centrum semiovale; LCWM, left cerebellar white matter.

in Glx precedes the drop in NAA, and that in WM, the drop in NAA precedes the drop in creatine. Myo-inositol and choline have a linear relationship to each other in the INCL patients, but appear to be unrelated in the reference group. Relative to NAA, both myo-inositol and choline initially rise as NAA drops, and later decline as NAA drops further. For choline, the initial rise occurs earlier in GM than in WM, and for myo-inositol, the late drop off occurs later in WM than in GM.

Statistical comparison between INCL and references

Metabolite ratios were tested for each anatomical location and also for combinations of locations reflecting WM, GM, and all locations together. The vast majority of comparisons were statistically significant at the $P \leq 0.05$ level. Of 80 comparisons, 69 met this cutoff, indicating that not only are the metabolite levels in INCL quantitatively different from the reference group, but also that their interrelationships are aberrant. The results of the statistical tests are presented in Table 3.

Discussion

In this study, we have performed serial quantitative ^{1}H-MRS measurements on two patients with INCL. The abnormalities appear to have started early in life (earlier than the age range covered by this study) and measurements for both patients followed roughly the same trajectory. Results at the different locations for different metabolites initially seem complicated, but are more easily interpreted if they are viewed as snapshots of two simultaneous temporal progressions – sequential involvement of the anatomical locations, and sequential abnormalities of the metabolites.

With regard to the spatial pattern, among the areas we measured, the PGM location is affected earliest and with greatest severity, and was already in a fairly advanced state by the time of our first measurement. Involvement of the LCSO and left thalamus trails the PGM only slightly; involvement of the LCWM lags behind the supratentorial structures and the pons is affected last among the locations we measured. Our findings are consistent with a previous report that alterations in metabolite ratios measured by ^{1}H-MRS can be observed as early as 3–5 months of age in the thalamus and parietal-occipital WM.[29]

The other observed progression is sequential abnormalities of the metabolites. Although INCL is a lysosomal storage disease that deposits S-acylated proteins (a constituent of ceroid) in the lysosomes of brain cells, it does not produce a product that is visible in a ^{1}H-MRS experiment at 3 T field strength. Therefore, we do not study the abnormal deposits directly, but rather we study their effects through changes in the normally visible metabolites that occur as a result of damage to the neurons and glia. We observed that the metabolites fell into two groups, according to their temporal pattern: a monophasic group (NAA, Glx, and creatine) whose levels declined as the disease progressed, and a biphasic group (myo-inositol and choline) whose levels initially rose and later fell.

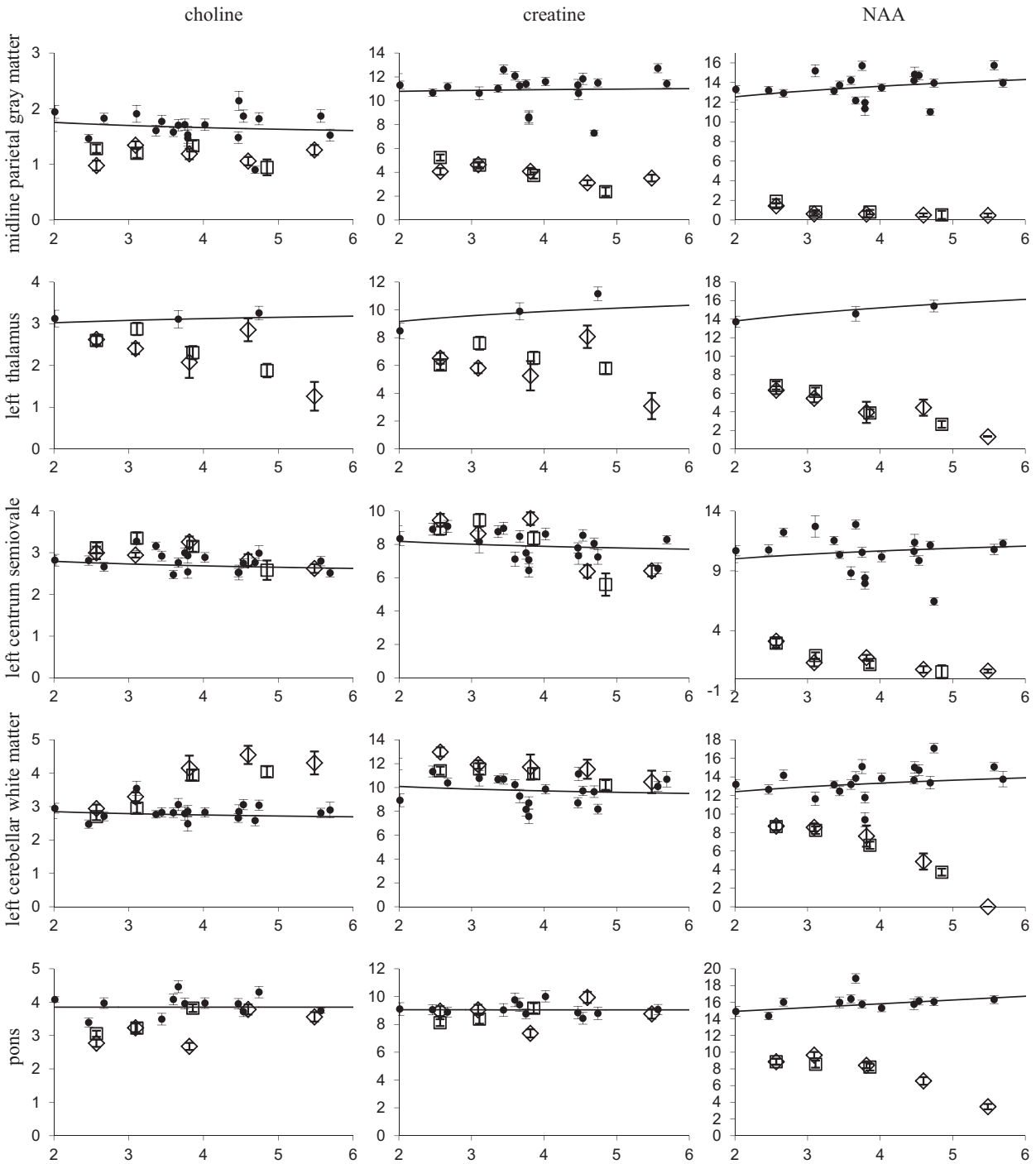

Figure 2. Comparison of INCL patients to the reference group. Squares and diamonds represent the individual INCL patients, while circles represent the reference group. These results have been corrected for the T2 of the metabolites. (Metabolite T2 in the INCL patients was up to 50% shorter than in the reference group, which if left uncorrected would systematically exaggerate a deficit in the patients relative to the references.) In the INCL patients, there is a clear deficit of NAA (left column) at all locations that progresses with time. There is a progressive deficit of creatine (middle column) in the two gray matter areas (thalamus and midline parietal gray matter). There is a progressive deficit of choline (left column) in the thalamus and progressive elevation of choline in the cerebellar white matter. There is a static deficit of choline in the midline parietal gray matter. On all plots, the horizontal axis is age (in years) and the vertical axis is tissue metabolite concentration (in mmol/L). INCL, infantile neuronal ceroid lipofuscinosis; NAA, *N*-acetylaspartate.

Table 2. NAA trajectory in the INCL patients.

Location	NAA as a function of age (using model with the best fit)	r^2
PGM	$y = 5.5826x^{-1.546}$	0.7531
LTHAL	$y = -1.6742x + 10.875$	0.9833
LCSO	$y = 22.43x^{-2.192}$	0.8888
LCWM	$y = -1.0932x^2 + 5.8932x + 0.6963$	0.9924
PONS	$y = -0.8626x^2 + 5.0618x + 1.61$	0.9769

NAA, *N*-acetylaspartate; INCL, infantile neuronal ceroid lipofuscinosis; PGM, parietal gray matter; LTHAL, left thalamus; LCSO, left centrum semiovale; LCWM, left cerebellar white matter.

The monophasic behavior of NAA and creatine, and the biphasic behavior of choline in INCL have been reported previously.[29]

At all locations, NAA was initially lower than normal and continued to drop throughout the follow-up period, falling below 1 mmol/L (effectively zero) earliest in the PGM, next in the LCSO, then in the left thalamus, and last in the LCWM. NAA in the pons did not fall below 1 mmol/L during the follow-up period. The pattern for Glx was similar to NAA, but with a delay in the onset of the pattern. The temporal pattern for creatine was initially normal in the early phases of the disease (pons and LCWM) and falling in the late phases of the disease (LCSO, left thalamus, and PGM).

In the locations we measured in the early phase of their involvement (pons and LCWM), we observed initially normal levels of myo-inositol and choline, and these rose later as the disease progressed. In the locations we measured in a more advanced phase (left thalamus and LCSO), myo-inositol was already high at our first measurement and started to decline by the end of the follow-up period, while choline had already peaked, and declined throughout the observation period. In the most advanced location (PGM), levels of both myo-inositol and choline were low and dropped slightly throughout the follow-up period.

Because the choline peak has contributions from multiple compounds performing various functions in the brain,[30] the meaning of an elevated choline peak depends upon the context; in INCL, the mechanisms that seem most likely to apply are either inflammation or gliosis (or both). Myo-inositol is a glia-specific marker[31] that is elevated by gliosis or inflammation.[32] The observed biphasic pattern (elevation followed by decline) suggests that there is an initial inflammatory phase, followed by a burn-out phase. This pattern follows what has been observed in the mouse model of INCL. In *Cln1*$^{-/-}$ mice[33] that recapitulate virtually all clinical pathological features of INCL[34] neuronal death is followed by infiltration of activated astrocytes and microglia. Recently, we generated another mouse model of INCL[35] by knocking-in the *Cln1* nonsense mutation (c.451C>T) most commonly found in the US INCL patient population. These mice also showed infiltration of activated astrocytes and microglia in the brain, which followed neuronal death. Thus, the results of our present study demonstrating elevated choline and myo-inositol in INCL patients are consistent with the results obtained from two different mouse models of INCL.

Decline of the monophasic metabolites would occur after the neurons accumulate a sufficient level of injury. NAA and NAAG are found mainly (or possibly exclusively) in neurons[30,36]; in clinical ^{1}H-MRS the NAA + NAAG peak is conventionally viewed as a marker of healthy neurons, and this peak decreases as neurons become unhealthy or die. Likewise the components of the Glx peak (predominantly neurotransmitters glutamate and GABA, and their metabolite glutamine) are produced by healthy glutamatergic neurons, GABA-ergic neurons, and astroglia (respectively), and drop when neurons die or are deprived of input.[37] The creatine peak includes both creatine and creatine phosphate; these compounds exchange high-energy phosphates with ATP and ADP, and serve as an intracellular reservoir of energy.[30] Thus, the creatine peak reflects intracellular energy stores and would be expected to drop only when there has been significant cell death per unit of tissue, and is thereby a lagging indicator of injury to neurons and glia.

It is well known that the T2 of water in the tissues changes as INCL progresses, as this is what brings about the widely reported abnormal signal seen on qualitative evaluation of T2-weighted MR images.[17,29,38,39] This observation should generate suspicion that metabolite T2 is also abnormal. Prediction of T2 in tissue is complicated and incompletely understood, but in general decreased water content, increased protein content, increased rigid-

Figure 3. Comparison of INCL patients to the reference group. Squares and diamonds represent the individual INCL patients, while circles represent the reference group. These results have not been corrected for the T2 of the metabolites. (Due to the complex nature of the mI and Glx peaks, the T2 could not be estimated from the data we collected. If mI and Glx follow the pattern of Cho, Cr, and NAA, then not correcting for a shorter T2 would exaggerate deficits and minimize elevations.) The pattern of myo-inositol appears to follow a temporal sequence of being initially normal, followed by elevation and then decline, with the sequence playing out earliest in the parietal gray matter, followed by the thalamus and centrum semiovale, then the cerebellar white matter, and last in the pons. The deficits of Glx parallel the deficits of NAA that are shown in Figure 1. On all plots, the horizontal axis is age (in years) and the vertical axis is tissue metabolite concentration (in mmol/L). INCL, infantile neuronal ceroid lipofuscinosis; mI, myo-inositol; Glx, glutamine + glutamate + GABA; Cho, choline; Cr, creatine; NAA, *N*-acetylaspartate.

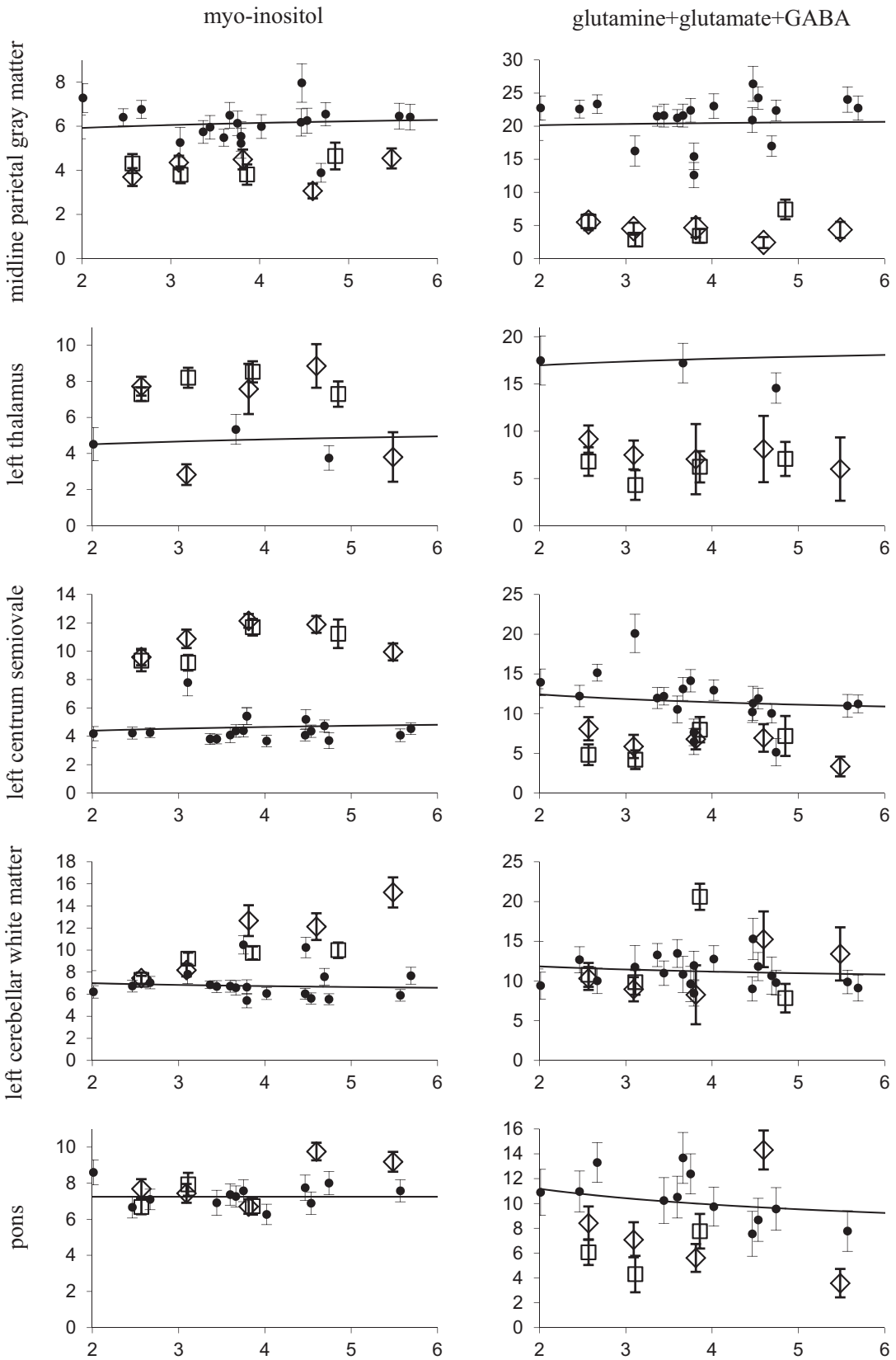

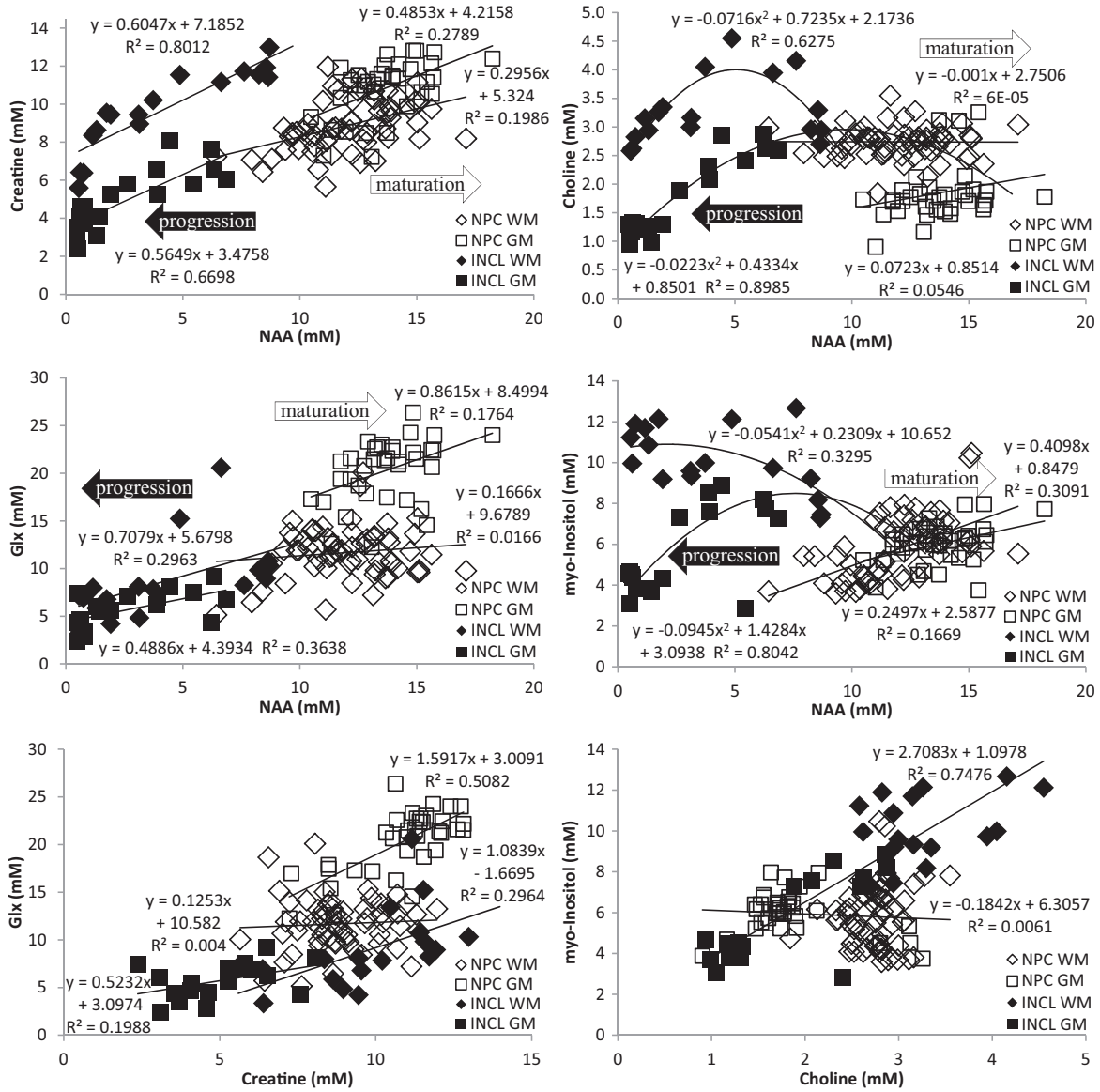

Figure 4. Relationships between the metabolites. Upper left: The relationship between creatine and NAA is linear. In white matter, the fit for INCL does not project into the reference cluster, suggesting that creatine in the WM persists for a while after the NAA starts dropping. Middle left: The relationship between Glx and NAA is linear. In gray matter, the fit for INCL does not project into the reference cluster, suggesting that loss of Glx precedes loss of NAA. Lower left: the relationship between creatine and Glx is also linear, and the timing pattern is consistent with the other two plots. Upper right: In the reference group, choline seems independent of NAA in the WM and weakly correlated in the GM, with a generally higher choline in the WM than in the GM. In INCL, the choline initially rises and later falls as the disease progresses, with GM leading WM (quadratic fits are shown, although other models may be better). Middle right: There is a weak linear correlation between myo-inositol and NAA in the reference group, with myo-inositol in the WM and GM essentially equal. In INCL, GM and WM deviate from normal at about the same time, but GM progresses faster into the falling phase. Lower right: In the reference group, choline and myo-inositol appeared to be independent of one another; choline was higher in WM than GM, while myo-inositol was about the same. In INCL, there was a strong linear relationship between choline and myo-inositol, which were both elevated in white matter. NAA, *N*-acetylaspartate; INCL, infantile neuronal ceroid lipofuscinosis; WM, white matter; Glx, glutamine + glutamate + GABA; GM, gray matter.

ity, and increased organization on a molecular level (such as in deposits) all lead to shortening of T2.[40] Metabolite T2 must be taken into account if accurate measurement of metabolite levels is desired.

Three metabolites (NAA, Glx, creatine) have a linear relationship to each other and monotonically decrease throughout the observed course of the disease. The order of involvement appears to be Glx before NAA (in

Table 3. Metabolite concentration ratios, *t*-test of INCL compared to reference.

Anatomical location	mI / NAA	Glx / NAA	Cr / NAA	Cho / NAA	mI / Cho	Glx / Cho	Cr / Cho	mI / Cr	Glx / Cr	mI / Glx
LCSO	0.002	0.008	<0.001	0.001	<0.001	<0.001	*0.056*	<0.001	<0.001	<0.001
LCWM	0.006	0.026	0.001	0.010	*0.058*	0.030	*0.293*	*0.062*	*0.321*	0.018
LTHAL	0.001	*0.117*	0.001	<0.001	<0.001	0.002	0.040	<0.001	0.037	0.001
PGM	<0.001	0.004	<0.001	<0.001	*0.411*	<0.001	<0.001	0.002	0.032	<0.001
PONS	*0.011*	*0.130*	0.005	0.017	0.001	*0.066*	0.004	0.051	0.004	0.019
LCSO&LCWM	0.002	0.004	<0.001	0.001	<0.001	<0.001	*0.100*	<0.001	<0.001	<0.001
LTHAL&PGM	<0.001	0.005	<0.001	<0.001	*0.392*	<0.001	<0.001	<0.001	<0.001	<0.001
ALL	<0.001	<0.001	<0.001	<0.001	<0.001	<0.001	<0.001	<0.001	<0.001	<0.001

Results with $P > 0.05$ are in smaller italic type. INCL, infantile neuronal ceroid lipofuscinosis; mI, myo-inositol; Glx, glutamine + glutamate + GABA; Cr, creatine; Cho, choline; NAA, *N*-acetylaspartate; LCSO, left centrum semiovale; LCWM, left cerebellar white matter; LTHAL, left thalamus; PGM, parietal gray matter.

GM) and NAA before creatine (in WM). Due to these properties, any of these metabolites could serve as a biomarker for disease progression and response to treatment; however NAA has the best SNR (and smallest measurement uncertainty), making NAA the best choice. Although the SNR is also fairly good in creatine, unlike NAA, creatine is not found exclusively in neurons, and therefore at low measured creatine, the measurement mainly reflects creatine found in cells other than neurons (such as glia) and ceases to be a good estimate of neuron viability. The two biphasic metabolites (myo-inositol and choline) are both well-known to be elevated in the context of inflammation. While a single measurement of the level of either of these metabolites does not indicate a unique point in the progression of the disease, it is a helpful indicator of the level of inflammation. In theory, metabolite T2 could be used as a biomarker for disease progression as well; however, T2 is a less practical biomarker than metabolite levels due to the greater uncertainty in the measurements.

Some limitations apply to this study. There are several issues related to estimation of metabolite T2. Late in the disease when metabolite levels are low, SNR is poor at long TE, causing greater uncertainty in the T2 estimates; attempting to improve SNR using more NEX has a heavy time cost, while attempting to improve SNR using only short TE measurements is mathematically suboptimal (error optimization requires separation of the first and last TE by roughly $1.25 \times T2$[41]). Correction for the T2 decay of multiplet peaks is challenging, because J-coupling results in a complicated evolution of the signal with TE that is poorly described by a monoexponential model; "effective T2" could be estimated, but accurate modelling would require many more than the three measurements we performed.[42] When metabolite T2 in the disease state is shorter than normal, lack of T2 correction exaggerates deficits and minimizes elevations. Although they were minimally symptomatic, our use of children with a known metabolic disorder as a reference group probably leads to a slight underestimate of normal NAA, Glx, and creatine; if so, then the actual deficits of these metabolites in INCL may be slightly greater than what we have presented. Because other markers of inflammation are elevated in the brains of NPC patients,[43] the actual elevations of myo-inositol and choline we measured in INCL patients are probably underestimated by some degree. Our study would have benefitted from data acquired earlier in the course of the disease, but unfortunately unless a patient has an affected older sibling the diagnosis of INCL is seldom made until after symptomatic brain injury occurs. Nevertheless, our results provide a detailed quantitative ^{1}H-MRS measurements of metabolites, which may be used as a benchmark to compare the effects of future therapeutic interventions in INCL patients.

Conclusions

These results describing the progression of brain metabolite T2 and quantitative metabolite levels in INCL are distinctive and dramatic, and are consistent with other established mechanisms of the disease. Although our patients were under treatment, we have no previous quantitative MRS reports to compare to, and therefore we cannot evaluate whether our treatment had any effect on metabolite T2 or metabolite levels compared to the natural history of the disease. However, these metabolite measurements are quantitative and were performed in such a way that they should be platform independent and institution independent. Therefore the results of this study can serve as a reference point for comparing the effectiveness

of future intervention strategies to our current trial of combination cysteamine bitartrate and *N*-acetylcysteine therapy.

Acknowledgment

We thank the patients (and their families) who participated in this study. We thank the MR technologists who scanned the patients (Bonita Damaska, Mastaneh Owhadi, and Betty Wise), and F. D. Porter for the use of his patients as a reference group. This project was supported entirely through intramural funding at the NIH: INCL patients were studied under protocol 01-CH-0086 and NPC patients were studied under protocol 06-CH-0186.

Conflict of Interest

The authors report no conflicts of interest. The opinions or assertions contained herein are to be considered the private views of this author (S. W. L.) and are not to be construed as official or as reflecting the views of the Department of the Army or the Department of Defense.

References

1. Anderson GW, Goebel HH, Simonati A. Human pathology in NCL. Biochim Biophys Acta 2013;1832:1807–1826.
2. Mole SE, Williams RE, Goebel HH. The neuronal ceroid lipofuscinoses (Batten disease). Oxford: Oxford University Press, 2011. P. 444.
3. Haltia M. The neuronal ceroid-lipofuscinoses: from past to present. Biochim Biophys Acta 2006;1762:850–856.
4. Platt FM, Boland B, van der Spoel AC. The cell biology of disease: lysosomal storage disorders: the cellular impact of lysosomal dysfunction. J Cell Biol 2012;199:723–734.
5. Rider JA, Rider DL. Batten disease: past, present, and future. Am J Med Genet Suppl 1988;5:21–26.
6. Mink JW, Augustine EF, Adams HR, et al. Classification and natural history of the neuronal ceroid lipofuscinoses. J Child Neurol 2013;28:1101–1105.
7. Cotman SL, Karaa A, Staropoli JF, Sims KB. Neuronal ceroid lipofuscinosis: impact of recent genetic advances and expansion of the clinicopathologic spectrum. Curr Neurol Neurosci Rep 2013;13:366.
8. Warrier V, Vieira M, Mole SE. Genetic basis and phenotypic correlations of the neuronal ceroid lipofusinoses. Biochim Biophys Acta 2013;1832:1827–1830.
9. Schulz A, Kohlschutter A, Mink J, et al. NCL diseases – clinical perspectives. Biochim Biophys Acta 2013;1832:1801–1806.
10. Haltia M, Rapola J, Santavuori P. Infantile type of so-called neuronal ceroid-lipofuscinosis. Histological and electron microscopic studies. Acta Neuropathol 1973;26:157–170.
11. Vesa J, Hellsten E, Verkruyse LA, et al. Mutations in the palmitoyl protein thioesterase gene causing infantile neuronal ceroid lipofuscinosis. Nature 1995;376:584–587.
12. Vanhanen SL, Sainio K, Lappi M, Santavuori P. EEG and evoked potentials in infantile neuronal ceroid-lipofuscinosis. Dev Med Child Neurol 1997;39:456–463.
13. Goebel HH, Wisniewski KE. Current state of clinical and morphological features in human NCL. Brain Pathol 2004;14:61–69.
14. Santavuori P, Vanhanen SL, Sainio K, et al. Infantile neuronal ceroid-lipofuscinosis (INCL): diagnostic criteria. J Inherit Metab Dis 1993;16:227–229.
15. Zhang Z, Butler JD, Levin SW, et al. Lysosomal ceroid depletion by drugs: therapeutic implications for a hereditary neurodegenerative disease of childhood. Nat Med 2001;7:478–484.
16. Bavarsad Shahripour R, Harrigan MR, Alexandrov AV. N-acetylcysteine (NAC) in neurological disorders: mechanisms of action and therapeutic opportunities. Brain Behav 2014;4:108–122.
17. Levin SW, Baker EH, Zein WM, et al. Oral cysteamine bitartrate and *N*-acetylcysteine for patients with infantile neuronal ceroid lipofuscinosis: a pilot study. Lancet Neurol 2014;13:777–787.
18. Yanjanin NM, Velez JI, Gropman A, et al. Linear clinical progression, independent of age of onset, in Niemann-Pick disease, type C. Am J Med Genet B Neuropsychiatr Genet 2010;153B:132–140.
19. Provencher SW. Automatic quantitation of localized in vivo 1H spectra with LCModel. NMR Biomed 2001;14:260–264.
20. Srinivasan R, Sailasuta N, Hurd R, et al. Evidence of elevated glutamate in multiple sclerosis using magnetic resonance spectroscopy at 3 T. Brain 2005;128:1016–1025.
21. Baker EH, Basso G, Barker PB, et al. Regional apparent metabolite concentrations in young adult brain measured by (1)H MR spectroscopy at 3 Tesla. J Magn Reson Imaging 2008;27:489–499.
22. Horska A, Calhoun VD, Bradshaw DH, Barker PB. Rapid method for correction of CSF partial volume in quantitative proton MR spectroscopic imaging. Magn Reson Med 2002;48:555–558.
23. Horska A, Kaufmann WE, Brant LJ, et al. In vivo quantitative proton MRSI study of brain development from childhood to adolescence. J Magn Reson Imaging 2002;15:137–143.
24. Kadota T, Horinouchi T, Kuroda C. Development and aging of the cerebrum: assessment with proton MR spectroscopy. AJNR Am J Neuroradiol 2001;22:128–135.
25. Kimura H, Fujii Y, Itoh S, et al. Metabolic alterations in the neonate and infant brain during development:

evaluation with proton MR spectroscopy. Radiology 1995;194:483–489.
26. Kreis R, Ernst T, Ross BD. Development of the human brain: in vivo quantification of metabolite and water content with proton magnetic resonance spectroscopy. Magn Reson Med 1993;30:424–437.
27. Pouwels PJ, Brockmann K, Kruse B, et al. Regional age dependence of human brain metabolites from infancy to adulthood as detected by quantitative localized proton MRS. Pediatr Res 1999;46:474–485.
28. Lundbom N, Barnett A, Bonavita S, et al. MR image segmentation and tissue metabolite contrast in 1H spectroscopic imaging of normal and aging brain. Magn Reson Med 1999;41:841–845.
29. Vanhanen SL, Puranen J, Autti T, et al. Neuroradiological findings (MRS, MRI, SPECT) in infantile neuronal ceroid-lipofuscinosis (infantile CLN1) at different stages of the disease. Neuropediatrics 2004;35:27–35.
30. Miller BL. A review of chemical issues in 1H NMR spectroscopy: *N*-acetyl-L-aspartate, creatine and choline. NMR Biomed 1991;4:47–52.
31. Brand A, Richter-Landsberg C, Leibfritz D. Multinuclear NMR studies on the energy metabolism of glial and neuronal cells. Dev Neurosci 1993;15:289–298.
32. Bitsch A, Bruhn H, Vougioukas V, et al. Inflammatory CNS demyelination: histopathologic correlation with in vivo quantitative proton MR spectroscopy. AJNR Am J Neuroradiol 1999;20:1619–1627.
33. Gupta P, Soyombo AA, Atashband A, et al. Disruption of PPT1 or PPT2 causes neuronal ceroid lipofuscinosis in knockout mice. Proc Natl Acad Sci USA 2001;98:13566–13571.
34. Bible E, Gupta P, Hofmann SL, Cooper JD. Regional and cellular neuropathology in the palmitoyl protein thioesterase-1 null mutant mouse model of infantile neuronal ceroid lipofuscinosis. Neurobiol Dis 2004;16:346–359.
35. Bouchelion A, Zhang Z, Li Y, et al. Mice homozygous for c.451C>T mutation in Cln1 gene recapitulate INCL phenotype. Ann Clin Transl Neurol 2014;1:1006–1023.
36. Simmons ML, Frondoza CG, Coyle JT. Immunocytochemical localization of *N*-acetyl-aspartate with monoclonal antibodies. Neuroscience 1991;45:37–45.
37. Arckens L, Schweigart G, Qu Y, et al. Cooperative changes in GABA, glutamate and activity levels: the missing link in cortical plasticity. Eur J Neurosci 2000;12:4222–4232.
38. Vanhanen SL, Raininko R, Autti T, Santavuori P. MRI evaluation of the brain in infantile neuronal ceroid-lipofuscinosis. Part 2: MRI findings in 21 patients. J Child Neurol 1995;10:444–450.
39. Confort-Gouny S, Chabrol B, Vion-Dury J, et al. MRI and localized proton MRS in early infantile form of neuronal ceroid-lipofuscinosis. Pediatr Neurol 1993;9:57–60.
40. Gore JC, Kennan RP. Physical and physiological basis of magnetic relaxation. In: Stark DD, Bradley WG, eds. Magnetic resonance imaging. 3rd ed. St Louis, MO: Mosby, 1999. Pp. 33–39.
41. Fleysher L, Fleysher R, Liu S, et al. Optimizing the precision-per-unit-time of quantitative MR metrics: examples for T1, T2, and DTI. Magn Reson Med 2007;57:380–387.
42. Xin L, Gambarota G, Mlynarik V, Gruetter R. Proton T2 relaxation time of J-coupled cerebral metabolites in rat brain at 9.4 T. NMR Biomed 2008;21:396–401.
43. Cologna SM, Cluzeau CV, Yanjanin NM, et al. Human and mouse neuroinflammation markers in Niemann-Pick disease, type C1. J Inherit Metab Dis 2014;37:83–92.